Anomeric Effect in Halogenated Methanols: A Quantum Theory of Atoms in Molecules Study

ARTICLE *in* THE JOURNAL OF PHYSICAL CHEMISTRY A · JANUARY 2013

Impact Factor: 2.69 · DOI: 10.1021/jp310534x · Source: PubMed

3 AUTHORS, INCLUDING:

David Ferro-Costas
University of Vigo
13 PUBLICATIONS **32** CITATIONS
SEE PROFILE

Ricardo Mosquera
University of Vigo
144 PUBLICATIONS **1,806** CITATIONS
SEE PROFILE

THE JOURNAL OF PHYSICAL CHEMISTRY A

Article

pubs.acs.org/JPCA

Anomeric Effect in Halogenated Methanols: A Quantum Theory of Atoms in Molecules Study

David Ferro-Costas, Antonio Vila, and Ricardo A. Mosquera*

Departamento de Química Física, Universidade de Vigo, Facultade de Química, Lagoas-Marcosende s/n, 36310 Vigo, Galicia, Spain

Supporting Information

ABSTRACT: The quantum theory of atoms in molecules (QTAIM) has been used to analyze the *gauche* conformational preference of fluoromethanol and chloromethanol. The analysis of the total atomic population and localization and delocalization indices show trends that are not in line with the hyperconjugative explanation. Energy terms arising from the QTAIM partitioning have been obtained for fluoromethanol, revealing that (i) C−O interaction plays the most significant role in stabilizing the *gauche* rotamer and (ii) the summation of exchange terms (the only ones that could be related to hyperconjugation) has a smaller weight than electrostatic ones in the energy balance among *gauche*, *anti*, and *syn* conformations; however, they are far from being negligible.

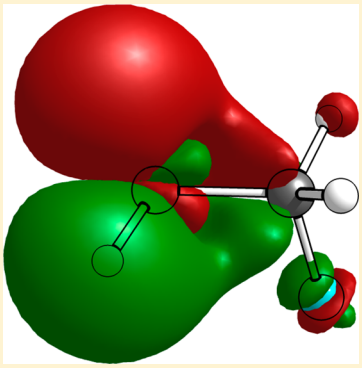

1. INTRODUCTION

The anomeric effect is one outstanding conformational feature of relevant chemical and biochemical compounds.[1−3] According to this effect, there is a conformational *gauche* preference of the R−A−B−X unit, where R represents an alkyl group (or hydrogen atom), A is an atom showing at least one lone pair (*lp*) of electrons, atom B bears a moderate electronegativity (like that of carbon), and X is an electronegative atom. Several explanations have been proposed to reveal the origin of the anomeric effect, and two of them have been widely accepted: (i) the electrostatic model, which basically compares the dipole−dipole interaction between A−R and B−X bonds in the different conformers of the molecule,[4,5] and (ii) the stereoelectronic model (SM),[6] which considers the presence of a favorable hyperconjugative interaction of one *lp* of A with an antibonding σ^* molecular orbital (practically centered in B and X atoms) in R−A−B−X *gauche* arrangements, frequently described as $n \rightarrow \sigma^*_{B-X}$ transferences or $R-A^+{=}B\cdots X^-$ resonance forms. The former model was soon found to be inadequate for explaining alone the conformational preferences of diverse systems, whereas the latter remains employed as it was originally proposed or combined with elements taken from other models, including the electrostatic one.[3]

Modern methods for the analysis of wave functions, like natural bond orbitals (NBO),[7] or even methods based on valence bond (VB) theories[8] and the analysis of electron densities, like the quantum theory of atoms in molecules (QTAIM),[9,10] have been also applied to account for the origin of the anomeric effect. NBO analysis has been generally found to support the presence of $n \rightarrow \sigma^*_{B-X}$ interactions combined with other terms, whose relative importance depends upon the molecular system.[11−14] However, the VB results[15] provide strong evidence that the $n \rightarrow \sigma^*_{B-X}$ interactions are not responsible for the anomeric effect and that it is better interpreted in terms of electrostatic interactions. In the same vein, the still scarce QTAIM studies[16−19] on this point also reveal facts that are not in line with the SM interpretation. On one hand, Werstiuk et al.[16] found that the conformational evolution of the Laplacian of the electron density values ($\nabla^2\rho$), related to oxygen lone pairs, is not compatible with a differential interaction of a *lp* with an antiperiplanar H_2C-O bond. On the other hand, previous work on the anomeric effect based on the results of four molecules with the O−C−O unit[17,18] and six containing the N−C−N unit[19] showed that bond properties evolve, along conformations, as could be predicted by the stereoelectronic model. Nevertheless, the conformational evolutions of delocalization indices (DIs)[20] and total atomic electron populations, $N(\Omega)$, cannot be interpreted in terms of larger (for the *gauche* R−A−B−X arrangement) and smaller (for the antiperiplanar one) $n \rightarrow \sigma^*_{B-X}$ interactions. In such manner, DIs remain practically unaltered along the conformational change or are even larger for conformations with antiperiplanar R−A−B−X arrangements, where the molecular geometry should allow no significant $n_X \rightarrow \sigma^*_{B-X}$ interactions.

Overall, according to previous works, NBO and QTAIM studies based on atomic integrated properties support different interpretations for the anomeric effect. As previously noticed, NBO and QTAIM analyses are based on different concepts. While the NBO origin arises from the analysis of bonding and antibonding MOs (obtained through a chosen unitary transformation of the whole set of MOs), the QTAIM origin is

Received: October 24, 2012
Revised: January 25, 2013
Published: January 25, 2013

   dx.doi.org/10.1021/jp310534x | *J. Phys. Chem. A* 2013, 117, 1641−1650

based on information provided by a physical observable, electron density (as other methods with chemical relevance, as "conceptual DFT"). Therefore, we should not forget that each explanation is reliable within the language developed for the concepts sustaining each model. It is up to each particular researcher to judge the reliability of them though. As an example of this controversial duality, the origin of the internal rotation barrier of ethane can be ascribed to steric hindrance[21] or to $\sigma-\sigma^*$ hyperconjugative interactions,[22] both of which are valid within the particular context of the model employed to derive the conclusions.

QTAIM partitioning can be used to create an energy decomposition scheme (see the next section) derived from the own terms of the electrostatic Hamiltonian. This offers a powerful tool, within this model, for inquiring into the physical origin of the anomeric effect. In this way, every conformational preference can be analyzed in terms of atomic and interatomic energies (instead of MO interactions, which offer a "true" origin in the NBO language). This partitioning was conducted for the simplest anomeric system, methanediol,[17] and for formic acid and other related molecules exhibiting a *Z* preference (an anomeric-like effect where B is an sp^2 carbon).[23] The results show that the *gauche* arrangement preference of the H−O−C−O moiety was mainly due to the 1,4-*gauche* stabilized interaction between oxygens and hydrogens (due to the enlargement of the O···H core attractions). The corresponding interaction was also found to be responsible for the *Z* stabilization of the H−O−C═O moiety.[23]

The anomeric effect has also been previously studied in fluoromethanol[24−28] and chloromethanol.[26−29] One of these works[25] includes a QTAIM analysis of fluoromethanol, and the authors claim, on the bases of local properties of the electron density $\rho(\mathbf{r})$, that the QTAIM results are in line with the SM. Therefore, we have thought that monohalogenated methanols could be of interest in checking our interpretation of the anomeric effect. Also, they are simple molecules in which the numerical calculation of electron−electron repulsions for each pair of basins is feasible at a rather moderate computational cost. Thus, this paper presents the results of the topological analysis of diverse conformations of fluoromethanol (**1**) and chloromethanol (**2**) aiming to explain the anomeric preferences in light of the QTAIM theory. Also, numerical calculation of the diverse terms of the atomic energy experienced within each atomic basin has been performed for molecule **1**.

2. METHODOLOGY

The *synperiplanar* (*s*), *gauche* (*g*), and *antiperiplanar* (*a*) conformations of molecules **1** and **2** were fully optimized at the HF, B3LYP, MP2, and CCSD levels using Gaussian 09[30] with the standard 6-311++G(2d,2p) 6d basis set. A relaxed potential energy scan (the dihedral of the anomeric moiety varying from 0° to 180° in steps of 20°) was also conducted to analyze the electron density of intermediate rotamers. It has been noticed previously that, to analyze the effects of stereoelectronic interactions, the role of geometry relaxation has to be decoupled from that of rigid rotations.[21] Thus, we have also computed an unrelaxed gauche geometry, **1*r***, obtained by rigid rotation from the optimized **1*a*** structure.

The integrations over the atomic basins of all the molecules were conducted using the AIMPAC program series.[31] The summation of integrated atomic electron populations and atomic energies yields the corresponding molecular properties within: 9×10^{-4} au and 0.5 kJ mol^{-1} for compound **1** and 1×10^{-3} au and 0.5 kJ mol^{-1} for compound **2**, respectively. The absolute values achieved for $L(\Omega)$ were always smaller than 9×10^{-4} au for **1** and 1×10^{-3} au for **2**. Similar values have been found to be sufficiently accurate in a large number of QTAIM papers. Also, as in other previous papers, we have found that HF, B3LYP, MP2, and CCSD calculations rendered, in what is our major concern (relative values between conformers), very similar results and unique conclusions (Figures S1 and S2 of the Supporting Information).

2.1. A QTAIM-Based Energy Partitioning for Anomeric Preference. The expected value for the molecular electronic energy, in the Born−Oppenheimer approximation, is given by eq 1

$$\langle \Psi|\hat{H}|\Psi\rangle = \sum_{i=1}^{N}\left\langle \Psi\left|-\frac{1}{2}\nabla_i^2\right|\Psi\right\rangle + \sum_{j=i+1}^{N}\sum_{i=1}^{N-1}\left\langle \Psi\left|\frac{1}{r_{ij}}\right|\Psi\right\rangle + \sum_{i=1}^{N}\sum_{\alpha=1}^{M}\left\langle \Psi\left|-\frac{Z_\alpha}{r_{i\alpha}}\right|\Psi\right\rangle + \sum_{\beta=\alpha+1}^{M}\sum_{\alpha=1}^{M-1}\frac{Z_\alpha Z_\beta}{r_{\alpha\beta}} \quad (1)$$

where Ψ is the wave function of the system, $\hat{H}$ is its Hamiltonian, r_{ij} is the distance between particles *i* and *j* (lowercase Greek letters are used, like α and β, for designing nuclei), Z_α is the charge of the α-nucleus, *M* is the number of nuclei, and *N* is the number of electrons.

When the Hartree−Fock wave function (Ψ_{HF}) is used, the electron−electron repulsion expectation value (V_{ee}, associated with the $1/r_{ij}$ operator) can be easily split (eq 2) into a term associated with the classical electron−electron repulsion between clouds of electron densities (V_{EE}) and another related to the exchange symmetry of indistinguishable particles (V_X):

$$\langle V_{ee}\rangle^{HF} = \sum_{j=i+1}^{N}\sum_{i=1}^{N-1}\left\langle \Psi_{HF}\left|\frac{1}{r_{ij}}\right|\Psi_{HF}\right\rangle = \sum_{j=i+1}^{N}\sum_{i=1}^{N-1}\langle V_{EE}\rangle_{ij}^{HF} + \sum_{j=i+1}^{N}\sum_{i=1}^{N-1}\langle V_X\rangle_{ij}^{HF} = \langle V_{EE}\rangle^{HF} + \langle V_X\rangle^{HF} \quad (2)$$

where the two-particle $\langle V_{EE}\rangle_{ij}^{HF}$ and $\langle V_X\rangle_{ij}^{HF}$ contributions are defined (eqs 3 and 4) in terms of the set of *N* spin molecular orbitals, $\{\chi_i\}$:

$$\langle V_{EE}\rangle_{ij}^{HF} = \left\langle \chi_i(1)\chi_j(2)\left|\frac{1}{r_{12}}\right|\chi_i(1)\chi_j(2)\right\rangle \quad (3)$$

$$\langle V_X\rangle_{ij}^{HF} = -\left\langle \chi_i(1)\chi_j(2)\left|\frac{1}{r_{12}}\right|\chi_j(1)\chi_i(2)\right\rangle \quad (4)$$

In addition, as $\langle V_{EE}\rangle_{ii}^{HF} + \langle V_X\rangle_{ii}^{HF}$ is equal to zero, the electron−electron repulsion can be split into classic electron−electron and exchange interactions where the self-interaction between electrons is considered, which is shown in eq 5 (indicated with the superscript s on V_{EE} and V_X).

$$\langle V_{EE}\rangle^{HF} + \langle V_X\rangle^{HF} = \sum_{j=i+1}^{N}\sum_{i=1}^{N-1}\{\langle V_{EE}\rangle_{ij}^{HF} + \langle V_X\rangle_{ij}^{HF}\} = \sum_{j=i}^{N}\sum_{i=1}^{N}\{\langle V_{EE}\rangle_{ij}^{HF} + \langle V_X\rangle_{ij}^{HF}\} = \langle V_{EE}^{s}\rangle^{HF} + \langle V_X^{s}\rangle^{HF} \quad (5)$$

dx.doi.org/10.1021/jp310534x | J. Phys. Chem. A 2013, 117, 1641−1650

Because of the deficiencies of the HF wave function, a correlation energy term (E_{corr}) has to be defined, to include the shortcomings of the HF wave function. In this manner, eq 1 turns into eq 6, where K is the kinetic energy, V_{ne} is the nucleus−electron (or core) attraction, and V_{nn} is the nucleus−nucleus repulsion.

$$\langle\Psi|\hat{H}|\Psi\rangle = \sum_{i=1}^{N}\langle K\rangle_i^{HF} + \sum_{j=i}^{N}\sum_{i=1}^{N}\{\langle V_{EE}\rangle_{ij}^{HF} + \langle V_X\rangle_{ij}^{HF}\} + \sum_{i=1}^{N}\sum_{\alpha=1}^{M}\langle V_{ne}\rangle_{\alpha i}^{HF} + \sum_{\beta=\alpha+1}^{M}\sum_{\alpha=1}^{M-1}\langle V_{nn}\rangle_{\alpha\beta}^{HF} + E_{corr} \quad (6)$$

This same energy partitioning, provided by the Hamiltonian itself when a HF wave function is considered, can be taken to the QTAIM context, splitting expected values into the corresponding atomic or diatomic contributions, computed for each atomic basin, Ω, or pair of basins, ΩΩ′, by integration of the corresponding density functions, which can be seen in eq 7, where M' is the number of QTAIM basins (usually equal to M).

$$\langle\Psi|\hat{H}|\Psi\rangle = \sum_{\Omega=1}^{M'}\langle K\rangle_\Omega^{HF} + \sum_{\Omega'=\Omega}^{M'}\sum_{\Omega=1}^{M'}\{\langle V_{EE}^s\rangle_{\Omega\Omega'}^{HF} + \langle V_X^s\rangle_{\Omega\Omega'}^{HF}\} + \sum_{\Omega=1}^{M'}\sum_{\alpha=1}^{M}\langle V_{ne}\rangle_{\alpha\Omega}^{HF} + \sum_{\beta=\alpha+1}^{M}\sum_{\alpha=1}^{M-1}\langle V_{nn}\rangle_{\alpha\beta}^{HF} + E_{corr} \quad (7)$$

The terms associated with the classic electron−electron repulsion and the exchange interaction between QTAIM basins Ω and Ω′ can be defined with and without self-interaction. In this case, we have chosen the former.

When $M' = M$ (the most usual situation), the different energy terms can be grouped. On one hand, via collection of all of the two-atom contributions, the total interatomic interaction energy between atoms associated with basins Ω and Ω′ (defined in the QTAIM context) is given by eq 8. On the other hand, the net energy of atom A is defined considering the kinetic energy of that atom and all the energy interactions that take place exclusively in the corresponding basin (eq 9).

$$V_{int}^{HF}(\Omega,\Omega') = \langle V_X^s\rangle_{\Omega\Omega'}^{HF} + \langle V_{EE}^s\rangle_{\Omega\Omega'}^{HF} + \langle V_{ne}\rangle_{\Omega\Omega'}^{HF} + \langle V_{ne}\rangle_{\Omega'\Omega}^{HF} + \langle V_{nn}\rangle_{\Omega\Omega'}^{HF} \quad (8)$$

$$E_{net}^{HF}(\Omega) = \langle K\rangle_\Omega^{HF} + \langle V_X^s\rangle_{\Omega\Omega}^{HF} + \langle V_{EE}^s\rangle_{\Omega\Omega}^{HF} + \langle V_{ne}\rangle_{\Omega\Omega}^{HF} \quad (9)$$

The introduction of these definitions into eq 7 yields eq 10, which is the chief equation in this energy partition scheme, similar to the one defined by Blanco et al.[32]

$$\langle\Psi|\hat{H}|\Psi\rangle = \sum_{\Omega} E_{net}^{HF}(\Omega) + \sum_{\Omega'>\Omega}^{M}\sum_{\Omega=1}^{M-1} V_{int}^{HF}(\Omega,\Omega') + E_{corr} \quad (10)$$

This energy partitioning (eq 10) is a useful tool for gaining insight into the physical origin of diverse processes, as it is based on the terms of the Hamiltonian and as atoms in the molecule are properly defined (all of this allowing one to gain, as a consequence, a real chemical comprehension of the system). Thus, the energy terms defined here have a clear physical meaning as they are based on well-defined operators.

The program STOCK[33] allowed us to obtain the terms of this QTAIM-based energy partitioning, integrating HF electron densities obtained for the completely optimized CCSD geometries. The correlation energy was estimated as the difference between the CCSD energy for the optimized structure and the single-point HF energy obtained for that geometry.

2.2. Localization and Delocalization Indices. The diagonal second-order reduced density matrix (2-RDM) is defined (using the McWeeny criteria for the normalization factor) according to eq 11

$$\Gamma(\vec{\mathbf{r}}_1,\vec{\mathbf{r}}_2) = N(N-1)\int d\vec{\mathbf{r}}_3...d\vec{\mathbf{r}}_N\,\Psi^*(\vec{\mathbf{r}}_1,\vec{\mathbf{r}}_2,\vec{\mathbf{r}}_3,...,\vec{\mathbf{r}}_N)\Psi(\vec{\mathbf{r}}_1,\vec{\mathbf{r}}_2,\vec{\mathbf{r}}_3,...,\vec{\mathbf{r}}_N) \quad (11)$$

where N is the number of electrons and $\mathbf{r}_i$ represents the spatial coordinates of electron i. Γ can be split into Coulomb and exchange correlation components:

$$\Gamma(\vec{\mathbf{r}}_1,\vec{\mathbf{r}}_2) = \Gamma_C(\vec{\mathbf{r}}_1,\vec{\mathbf{r}}_2) + \Gamma_{xc}(\vec{\mathbf{r}}_1,\vec{\mathbf{r}}_2) \quad (12)$$

defining the Coulomb part as the product $\Gamma_C(\mathbf{r}_1,\mathbf{r}_2) = \rho(\mathbf{r}_1)\cdot\rho(\mathbf{r}_2)$.

On the other hand, and in relation to the QTAIM, the localization and delocalization indices (LIs and DIs, respectively) arise from the exchange correlation component of the 2-RDM.[34] These are defined as $\lambda(A) = |F_{AA}|$ and $\delta(A,B) = |F_{AB}| + |F_{BA}|$, respectively, being

$$F_{AB} = \int_{\Omega_A} d\vec{\mathbf{r}}_1 \int_{\Omega_B} d\vec{\mathbf{r}}_2\,\Gamma_{xc}(\vec{\mathbf{r}}_1,\vec{\mathbf{r}}_2) \quad (13)$$

It is straightforward to obtain eq 14, which allows the electron population of a given basin Ω_A to be split into localized and delocalized parts.

$$F_{AA} + \sum_{B\neq A} F_{AB} = -N(\Omega_A) \quad (14)$$

Obtaining the Γ_{xc} for multideterminantal wave functions (as, for example, for CCSD wave functions) is, in general, far from trivial. However, there are some approximate 2-RDMs that are built in terms of the natural molecular orbitals (NMOs) and their occupation numbers. For instance, the Müller 2-RDM (or Buijse−Baerends functional)[35,36] is given by eq 15

$$\Gamma_{xc}(\vec{\mathbf{r}}_1,\vec{\mathbf{r}}_2) \cong -\sum_{i,j}(n_i n_j)^{1/2}\eta_i(\vec{\mathbf{r}}_1)\eta_j^*(\vec{\mathbf{r}}_1)\eta_i^*(\vec{\mathbf{r}}_2)\eta_j(\vec{\mathbf{r}}_2) \quad (15)$$

where n_i is the occupation number of the natural molecular orbital η_i. Using this functional, the DI between two basins, $\delta(A,B)$, takes the form

$$\delta(A,B) \cong 2\sum_{i,j}(n_i n_j)^{1/2}S_{ij}(A)S_{ij}(B) \quad (16)$$

$S_{ij}(A)$ being the overlap integral between η_i and η_j in the basin of atom A.

3. RESULTS AND DISCUSSION

3.1. Conformational Analysis and Geometries. Three different stationary points were obtained for **1** and **2** at the HF, B3LYP, MP2, and CCSD levels (Figures 1 and 2 and Figure S3 of the Supporting Information): *synperiplanar* (*c*), *gauche* (*g*), and *antiperiplanar* (*a*). Nevertheless, only the *gauche* conformation was confirmed as a true minimum by the vibrational frequency analysis, in agreement with all the previously reported computational studies. The molecular energies

dx.doi.org/10.1021/jp310534x | J. Phys. Chem. A 2013, 117, 1641−1650

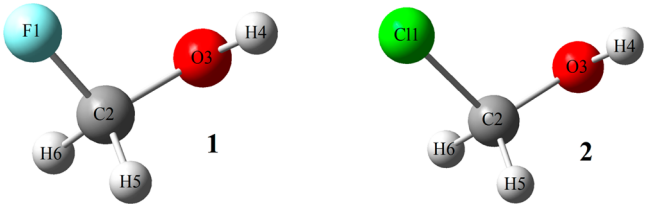

Figure 1. *Gauche* conformers (with atom numbering) of fluoromethanol (**1**) and chloromethanol (**2**).

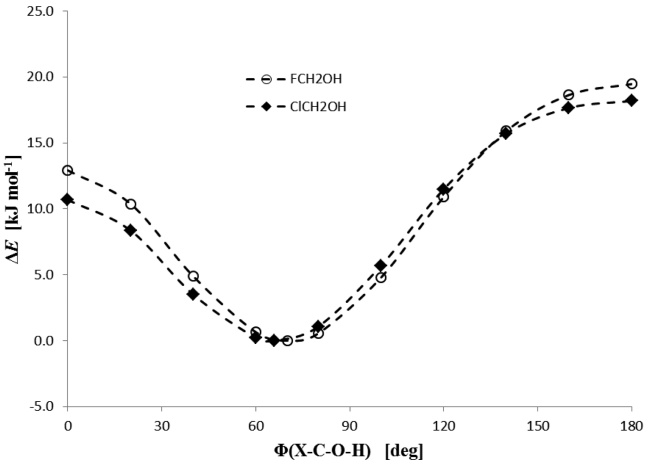

Figure 2. CCSD/6-311++G(2d,2p) 6d potential curve for internal rotation of the X−C−O−H moiety around the C−O bond in **1** (X = F) and **2** (X = Cl).

(relative to the true conformer, namely the *g* conformer) for **1** and **2** are listed in Table 1. As a benchmark calculation, we also report G2 relative energies. Unexpectedly, HF relative energies provide the best agreement with G2 ones. The anomeric stabilization in **1** and **2** is similar to that of dimethoxymethane [at the CCSD/6-311++G(2d,2p) 6d level, where the *gg* conformer is 25.1 kJ mol^{-1} more stable than the *tt* counterpart]. As one can observe, the replacement of F with Cl has little impact on the relative molecular energies (Figure 2).

The most pronounced geometrical changes along the internal rotation in **1** and **2** (from *a* to *c*) occur at the anomeric unit (Table S1 of the Supporting Information). Thus, we observe the characteristic signature of the anomeric effect: shortening of the C2−O3 bond, elongation of the X1−C2 bond (X = F for **1**, and X = Cl for **2**), and widening of the X1−C2−O3 bond angle on going from the *anti* to the *gauche* conformation. As could be anticipated on the basis of the difference in the size and electronegativity of the halogens, the Cl−C bond distance displays larger changes than the F−C one. Unfortunately, no experimental data are available for a comparison of geometrical parameters.

3.2. Atomic QTAIM Properties. According to the SM, the *gauche* stabilization in **1** is believed to arise from the delocalization of one oxygen *lp* into the σ^*_{C-F} orbital. As indicated in the Introduction, Roohi and Ebrahimi[25] reported conciliation between the predictions of the SM and QTAIM bond critical point (BCP) properties for fluoromethanol. Although we also noted in previous papers that the evolution of BCP properties was consistent with the geometrical signature of the anomeric effect, in our view it does not imply the existence of a stabilizing stereoelectronic interaction between an unshared *lp* at oxygen and (mainly) a B−X antibonding orbital. Furthermore, Perrin et al.[37] also concluded that the shortening of the polar A−B bond can be satisfactorily explained on the basis of electrostatic interactions. Therefore, the modification of the geometry is not a necessary and sufficient condition to invoke the SM model.

The evolution experienced by atomic electron populations, $\Delta N(\Omega)$, of molecule **1** along the internal rotation (plotted in Figure 3a, taking **1***a* as a reference; see also Table S2 of the

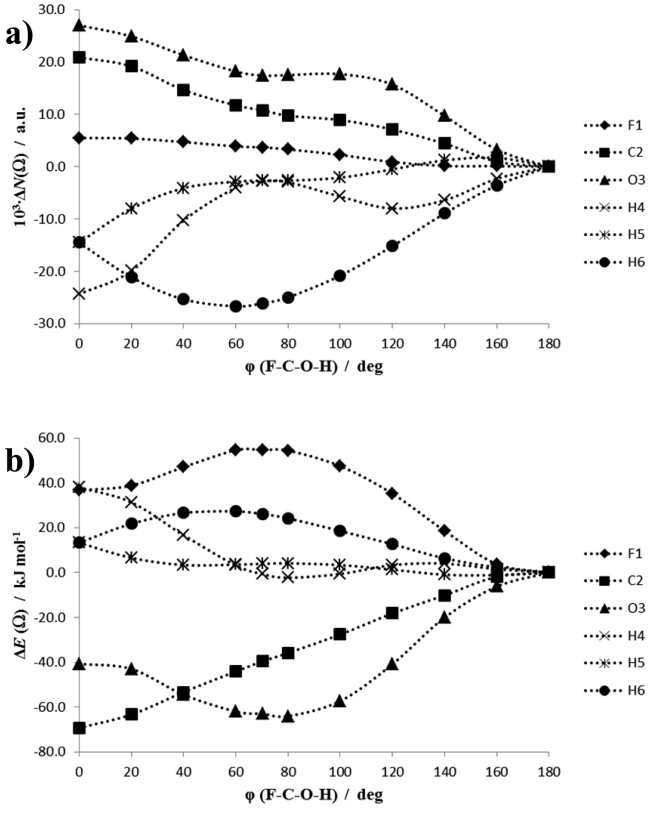

Figure 3. Evolution of atomic electron populations (a) and energies (b) along the internal rotation in fluoromethanol as integrated from CCSD/6-311++(2d,2p) 6d electron densities.

Table 1. Absolute (in atomic units for *g* conformers) and Relative (in kilojoules per mole for *a* and *c* conformations) Energies for the Stationary Points of Fluoromethanol (1) and Chloromethanol (2)

	1*g*	1*a*	1*c*	2*g*	2*a*	2*c*
HF/6-311++G(2d,2p) 6d	−213.98442	17.8	10.6	−574.02194	18.1	9.8
B3LYP/6-311++G(2d,2p) 6d	−215.05342	20.6	13.5	−575.40453	21.5	12.3
MP2/6-311++G(2d,2p) 6d	−214.59609	20.5	13.8	−574.56192	19.2	11.1
CCSD/6-311++G(2d,2p) 6d	−214.60760	19.5	12.9	−574.58629	18.2	10.7
G2	−214.70199	16.5	10.8	−574.69156	14.7	8.4

dx.doi.org/10.1021/jp310534x | J. Phys. Chem. A 2013, 117, 1641−1650

Table 2. Relative Atomic Basin Delocalization Indices $\Delta\delta(\Omega,\Omega')$ (with regard to 1*a*) in 1*g* and 1*r* (in parentheses), from CCSD/6-311++(2d,2p) 6d Electron Densities, Obtained through the Müller 2-RDM[a]

	F1	C2	O3	H4	H5	H6	$\Delta N^{del}(\Omega)$
F1	8.0 (10.5)						−4.2 (6.2)
C2	−7.6 (−6.1)	6.3 (17.0)					4.6 (0.5)
O3	7.3 (23.8)	13.9 (2.7)	11.6 (−0.4)				6.0 (3.7)
H4	−5.7 (−4.8)	1.1 (1.1)	−5.9 (−6.4)	−0.9 (−1.6)			−1.9 (−2.0)
H5	1.2 (1.3)	1.4 (1.6)	1.9 (0.5)	1.0 (0.9)	−3.8 (−2.5)		1.2 (1.0)
H6	−3.7 (−1.9)	0.3 (1.7)	−5.2 (−13.2)	5.7 (5.0)	−3.0 (−2.3)	−23.2 (−26.5)	−2.9 (−5.3)

[a]In the last column, the relative delocalized electron population for each basin, $\Delta N^{del}(\Omega)$, is given. All the values are in atomic units and multiplied by 10^3.

Supporting Information) is not consistent with the predictions of the SM. According to this model, if the delocalization of one oxygen *lp* into the C−F nonbonding orbital is the "dominant" stereoelectronic effect, ΔN(O3) should be negative for **1*g***, whereas ΔN(C2) and ΔN(F1) should display positive values for this conformation. Nevertheless, our calculations yielded positive ΔN(O3) values upon progressive rotation from the *antiperiplanar* arrangement, with a relative value of 0.017 au in **1*g*** (respect to **1*a***). In fact, ∼33% of the electron population increase in the oxygen basin takes place over the delocalized part [the localized increases in 0.012 au and the delocalized one in 0.006 au (Table 2)]. Moreover, the volume of the oxygen atomic basin (limited by the 0.001 au contour) has little impact on this variation: it decreases only marginally by 0.1 au in the *gauche* conformation (this volume, for the oxygen basin, in the *gauche* arrangement is 122.3 au). It is also important to remark that an important amount of electron density flows from C2 to O3 (Figure 4), instead of the O3 to C2 flux predicted by SM. This indicates that if the $n_O \rightarrow \sigma^*_{C-F}$ interaction exists, it is not dominant.

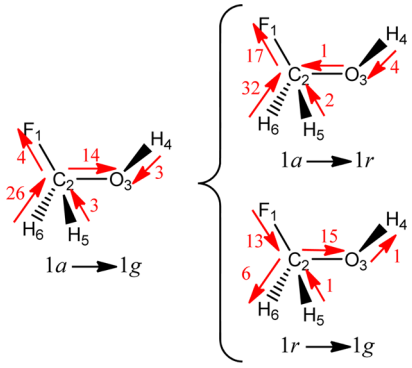

Figure 4. Electron density reorganizations (in atomic units multiplied by 10^3) accompanying the conformational interconversion (from **1*a*** to **1*g*** and also from **1*a*** to **1*r*** and from **1*r*** to **1*g***, CCSD level).

The largest variation (from **1*a*** to **1*g***) in atomic population upon rotation around the C−O bond occurs for H6 (Figures 3 and 4), more notable than those of C2 and O3. The fluorine atomic population remains virtually unaltered, as could be expected from its high electronegativity. These observations are congruent with the results of our previous work on the anomeric effect in the O−C−O[17,18] and N−C−N[19] units, as indicated in the Introduction. The differing behavior of the atomic populations of the two hydrogens attached to carbon (these are H5 and H6) can be related to their *gauche* interactions with the *lps* at oxygen. Thus, in **1*a***, both hydrogens display one *gauche* interaction with oxygen *lps*; upon rotation to yield **1*g***, H6 becomes *gauche* to the two *lps*, whereas H5 is only *gauche* to one of the *lps* (Figure 5). In other words, the stepwise

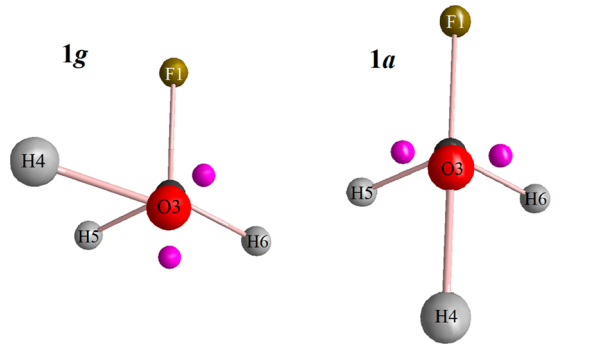

Figure 5. (3,+3) critical points of $\nabla^2\rho(\mathbf{r})$ associated with the oxygen lone pairs (lilac spheres) for the **1*g*** and **1*a*** conformations.

electron population decrease of H6 on going from **1*a*** to **1*g*** can be interpreted as a result of increased electrostatic repulsions with oxygen *lps*. As shown in Table S4 (Supporting Information), rotation away from the *anti* conformation brings the H6 nucleus (and its atomic basin) closer to one of the oxygen *lps*, whereas the variation of distance to the other *lp* is much smaller. On the other hand, upon rotation H5 approaches one of the *lps*, whereas it moves away from the other one. As a consequence, the internal rotation has little impact on *N*(H5) and an important effect on *N*(H6). In the same vein, the atomic electron population of hydroxylic H4 is only significantly affected when it approaches the *synperiplanar* arrangement to fluorine (Figure 3a). It is also important to note the progressive character of these variations with the internal rotation of the F−C−O−H moiety (Figure 3a).

Rigid rotation around the C−O bond from **1*a*** to the *gauche* arrangement, **1*r*** (6.2 kJ mol^{-1} higher in energy than **1*g***), reveals the depletion of the H6 atomic population is mainly induced by the rotation (Figures 4 and 6) and not by a subsequent nuclear reorganization due to the full optimization. Thus, the **1*r*** relative atomic populations of the atoms (in atomic units and multiplied by 10^3) are 17, 17, 3, −4, −2, and −32 from F1 to H6, respectively. We notice that (i) the electron density transfer through the C−O bond takes place in the same direction predicted by the SM (from O3 to C2), (ii) the magnitude of this transfer is negligible (around 1×10^{-3} au), and (iii) despite the fact that the C−O bond shrinks in **1*r*** → **1*g*** (so a larger $n_0-\sigma^*_{C-F}$ overlap is expected) the electron transference along this bond takes the opposite direction. Overall, in terms of total atomic electron populations, the **1*r*** → **1*g*** step results basically in transferring, from F1 to O3, the electron density sent previously along the rigid rotation from

dx.doi.org/10.1021/jp310534x | J. Phys. Chem. A 2013, 117, 1641−1650

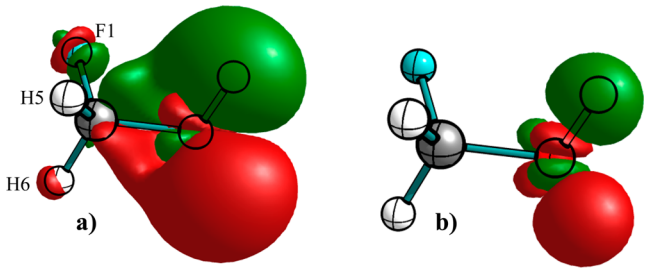

Figure 6. $\Delta\rho(\mathbf{r}) \pm 0.003$ au (a) and ± 0.03 au (b) isosurfaces for the **1*a*** → **1*r*** step. Green color is associated with positive values and red with negative ones. The depletion around H6 upon rigid rotation to the *gauche* arrangement can be observed (a), while the H5 environment remains nearly constant.

H6 to F1. Thus, the *a priori* expected constancy of N(F) for the **1*a*** → **1*g*** step is not due to its high electronegativity but the result of two combined effects.

3.3. Electron Delocalization. As described in section 3.2, electron delocalization between pairs of basins plays an important role in the increase in the oxygen electron population of **1*g*** relative to that of **1*a***. Thus, O3 shares more electron density with carbon and fluorine atomic basins in the *gauche* conformation (Table 2). Considering the structure of **1*r***, we notice that rigid rotation (from **1*a***), where the distance among these three atoms is exactly the same and the arrangement of oxygen *lp*s and hydroxylic H with regard to the C−F bond has changed, increases by a larger amount the electron density of O shared with F (0.024 au) than that shared with C (0.003 au). It has to be noticed that the reverse sequence would be the one expected for an electron density transference from one O *lp* to a σ^*_{C-F} MO, where the antibonding character predicts larger coefficients for the primitives centered on the least electronegative atom (in this case, the C). Additionally, the evolution of δ(F1,O3) and δ(C2,O3) from **1*r*** to **1*g*** is in accordance with the evolution of the interatomic distance.

3.4. *Gauche* Stabilization. The results obtained from the QTAIM-based energy partition (Table 3) show that the stabilization of **1*g*** relies, basically, on the total interaction between C2 and O3. Moreover, this interaction is more important than that involving the F1−H4 pair (2.6 times larger), contrary to what could be expected using methanediol as a model.[17,23] Furthermore, F1 and C2 atomic net energies also play a role in **1*g*** stabilization, comparable with that of F1−H4 total interaction.

We notice that the largest **1*a*** → **1*g*** variation, ΔV_T(C2,O3), involves the two basins displaying the most negative $\Delta E(\Omega)$ values (Figure 3b; see also Table S3 of the Supporting Information). Although no $\Delta V_X(\Omega)$ or $\Delta V_X(\Omega,\Omega')$ values seem to be remarkable (Table S5 of the Supporting Information), when all of them are summed for the whole molecule, we realize the summation of electrostatic contributions (−27.6 kJ mol^{-1}) is <6 times larger than that of exchanges (−5.2 kJ mol^{-1}). According to the concept of electron delocalization usually described in general organic chemistry books, only the exchange terms of the energy could be related with this effect. However, it is important to remark that other "concepts" could be part of these exchange terms, and the trends in V_X cannot be totally related to hyperconjugative effects. Thus, although electron delocalization seems not to be the main reason for *gauche* stabilization, their role could be not negligible according to our model. Nevertheless, this includes the effect of all kinds of electron delocalizations, not only the $n_O \rightarrow \sigma^*_{C-F}$ one. Moreover, the relative unimportance of delocalization between O and the C−F bond could be traced by other properties within the QTAIM framework as previously discussed.

To improve our understanding of the **1*a*** → **1*g*** process, we have split it into two steps: (i) the rigid rotation, **1*a*** → **1*r*** (Table 4), and (ii) the reorganization of the nuclei in the *gauche* arrangement, **1*r*** → **1*g*** (Table 5). Thus, during the rigid rotation, the energy of the *gauche* arrangement (**1*r***) is smaller (−13.2 kJ mol^{-1}) than that of **1*a***, basically, because of two energy terms: F1−H4 interaction and C2 net energy. The other two terms (F1 and C2−O3) increase in the reorganization of the nuclei (−6.2 kJ mol^{-1}). According to the QTAIM-based energy partitioning, the stabilization of E_{net}(F1) lies on the depletion of the electron population of the highly negative F basin in the **1*r*** → **1*g*** step, which weakens the electron−electron repulsion in its own basin and the atomic electron kinetic energy, while the origin of the other three relies on the enlargement of core attractions.

$\Delta V_X(\Omega)$ and $\Delta V_X(\Omega,\Omega')$ terms (Tables S6 and S7 of the Supporting Information) for the rigid rotation total −9.6 kJ mol^{-1}, while the electrostatic terms sum to −38.7 kJ mol^{-1}, revealing the contribution of electronic exchange is indeed larger when nuclear relaxation is not included. Moreover, the exchange energy between O and C−F units [V_X(F1,O3) + V_X(C2,O3)] accounts −12.9 kJ mol^{-1} more in **1*r*** than in **1*a*** (Table S6 of the Supporting Information), while it accounts for only −0.6 kJ mol^{-1} in the nuclear reorganization (Table S7 of the Supporting Information). That is, FC···O bond delocalization has larger energy effects in rigid rotations than in nuclear reorganization. In contrast, the variation of the classic electrostatic interaction between O and the F−C bond is smaller in the rigid rotation (21.2 kJ mol^{-1}) than in the nuclear

Table 3. Relative QTAIM-Based Energy Terms for 1*g* with Regard to 1*a* (in kilojoules per mole), According to Equation 10[a]

	$\Delta V^{HF}_{int}(i,j)$							
	F1	C2	O3	H4	H5	H6	$\Delta E^{HF}_{net}(j)$	ΔE_{corr}
F1							−35.6	
C2	89.7						−39.2	
O3	27.8	−106.8					48.8	
H4	−41.2	37.6	−14.4				5.2	
H5	−0.6	1.5	−4.2	0.7			0.3	
H6	−11.6	37.4	−26.1	9.2	1.9		1.7	
FCH_2OH								−1.9

[a]The second row lists *i* atoms and the first column *j* atoms.

dx.doi.org/10.1021/jp310534x | J. Phys. Chem. A 2013, 117, 1641−1650

Table 4. Relative QTAIM-Based Energy Terms for 1*r* with Regard to 1*a* (in kilojoules per mole), According to Equation 10[a]

	$\Delta V_{int}^{HF}(i,j)$							
	F1	C2	O3	H4	H5	H6	$\Delta E_{net}^{HF}(j)$	ΔE_{corr}
F1							14.7	
C2	18.4						−52.5	
O3	26.6	−18.3					6.9	
H4	−51.7	29.7	−5.0				5.9	
H5	−0.4	−0.7	−1.4	0.1			−0.1	
H6	−17.7	43.7	−22.5	10.7	1.8		−0.7	
FCH_2OH								−0.5

[a]The second row lists *i* atoms and the first column *j* atoms.

Table 5. Relative QTAIM-Based Energy Terms for 1*g* with Regard to 1*r* (in kilojoules per mole), According to Equation 10[a]

	$\Delta V_{int}^{HF}(i,j)$							
	F1	C2	O3	H4	H5	H6	$\Delta E_{net}^{HF}(j)$	ΔE_{corr}
F1							−50.3	
C2	71.3						13.3	
O3	1.2	−88.5					42.0	
H4	10.4	7.9	−9.4				−0.7	
H5	−0.2	2.2	−2.8	0.6			0.4	
H6	6.0	−6.3	−3.6	−1.5	0.1		2.4	
FCH_2OH								−1.4

[a]The second row lists *i* atoms and the first column *j* atoms.

Table 6. Relative QTAIM-Based Energy Terms for 1*c* with Regard to 1*a* (in kilojoules per mole), According to Equation 10[a]

	$\Delta V_{int}^{HF}(i,j)$							
	F1	C2	O3	H4	H5	H6	$\Delta E_{net}^{HF}(j)$	ΔE_{corr}
F1							−18.3	
C2	70.8						−66.8	
O3	47.1	−52.4					28.8	
H4	−96.1	79.5	−45.3				29.1	
H5	−6.5	19.0	−14.5	7.3			1.3	
H6	−6.5	19.0	−14.5	7.3	1.6		1.3	
FCH_2OH								0.6

[a]The second row lists *i* atoms and the first column *j* atoms.

Table 7. Relative QTAIM-Based Energy Terms for 1*g* with Regard to 1*c* (in kilojoules per mole), According to Equation 10[a]

	$\Delta V_{int}^{HF}(i,j)$							
	F1	C2	O3	H4	H5	H6	$\Delta E_{net}^{HF}(j)$	ΔE_{corr}
F1							−17.3	
C2	18.9						27.6	
O3	−19.3	−54.4					20.0	
H4	54.8	−41.9	30.9				−23.8	
H5	5.9	−17.5	10.3	−6.6			−1.0	
H6	−5.2	18.4	−11.5	1.9	0.3		0.3	
FCH_2OH								−2.5

[a]The second row lists *i* atoms and the first column *j* atoms.

reorganization (−86.7 kJ mol^{-1}). This discussion could be considered to be consistent with the fact that hyperconjugative interactions experienced along rigid rotation are hidden by other energy terms after nuclear relaxation. Nevertheless, along the rigid rotation, the atom pairs involved in the $n_O \rightarrow \sigma^*_{C-F}$ delocalization do not display the largest $\Delta V_{int}(i,j)$ for the process (Table 4).

3.5. *Anti* versus *Syn* Arrangement. The interconversion between *gauche* conformers can also take place through **1*c*** (**1*g*** → **1*c*** → **1*g***), experiencing a lower energy barrier than through **1*a*** (Figure 2). Which interaction(s) makes the energy of **1*c*** smaller than that of **1*a***? The answer can be obtained, once again, through QTAIM-based energy partitioning. According to data in Table 6, the stabilization of **1*c*** with regard to **1*a*** arises, basically, from the following terms (from largest to smallest, in absolute values): V_T(F1,H4), E_{net}(C2), V_T(C2,O3), and V_T(O3,H4). In this case, the most important one is the total interaction between the fluorine and the hydroxyl hydrogen (due, basically, to the core attraction energies). We want to highlight this fact is consistent with the results obtained for

dx.doi.org/10.1021/jp310534x | J. Phys. Chem. A 2013, 117, 1641−1650

methanediol and formic acid. In such a way, the behavior of **1*c*** with respect to that of **1*a*** could be inferred from previous studies of the anomeric effect[17] and Z preference.[23]

On the other side, one of the most significant changes experienced by energy terms during the **1*c*** → **1*g*** interconversion corresponds to V_T(F1,H4), as it could be expected from the variation of internuclear distances (Table 7). Nevertheless, the amount of variation experienced by V_T(C2,O3) and V_T(C2,H4) is nearly equivalent (each one) to that of V_T(F1,H4), counteracting its destabilizing effect. In these cases, the origin is related not only to internuclear distances but also to the increase in the population within the H4 basin.

3.6. Chloromethanol. The analysis and explanation described above can be applied *mutatis mutandis* to the chlorine analogue. Panels a and b of Figure 7 show a plot of the variations of atomic populations and energies, respectively, upon rotation from the *anti* conformation. Relative to the *anti* conformation, N(H6) decreases 0.026 au, as in fluoromethanol. However, in this case, the smaller electronegativity of the halogen results in an increase in the level of participation of all the atoms in the electron density redistribution. Thus, H6 does not display the largest variation of atomic charge, as in the fluorine analogue. Taking the *anti* conformation as the reference state, we found the electron population flows toward the chlorine (0.058 au) and to a lesser extent to the oxygen (which increases its total electron population to 0.019 au), whereas the carbon becomes less populated (−0.037 au). As with the fluorine analogue, the loss of electronic charge in H6 can be related to the approach of this atom toward the oxygen *lps*. In contrast to the fluorine analogue, the halogen atom withdraws a considerable amount of electron population, despite the fact that the fluorine atom is substantially more electronegative (according to the Allred−Rochow scale fluorine has an electronegativity of 4.10, whereas the value for chlorine is 2.83). Regardless, these results can be rationalized on the basis of the larger polarizability of the chlorine atom with regard to the fluorine atom.

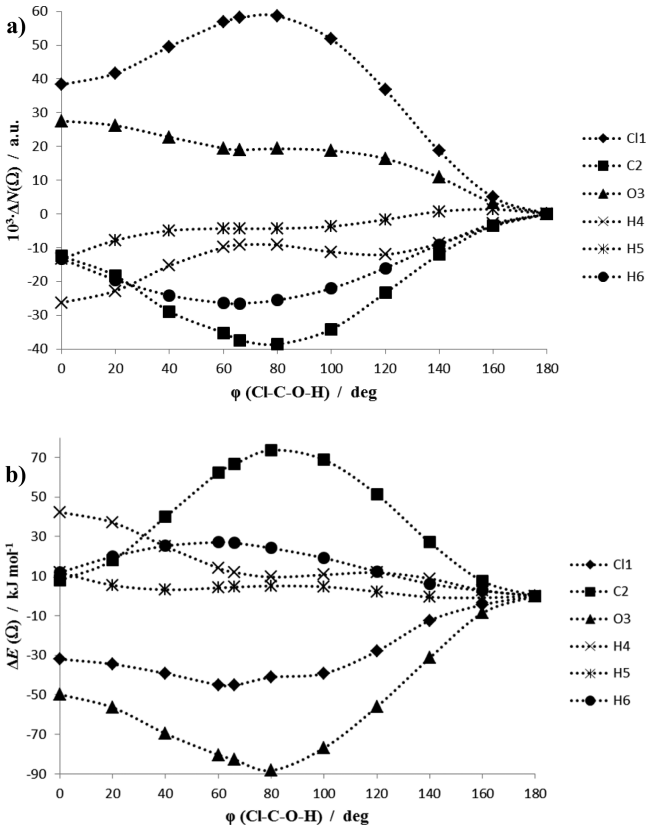

Figure 7. Evolution of atomic electron populations (a) and energies (b) along the internal rotation in chloromethanol as integrated from CCSD/6-311++(2d,2p) 6d electron densities.

Variations in DIs during the conformational interconversion (Table 8) follow the same pattern described above for fluoromethanol. Thus, δ(Cl1,C2) decreases in **2*g*** as a result of the Cl1−C2 bond becoming longer. The larger N(Cl1) value for **2*g*** explains why λ(Cl1) increases. Once again, the enlargement of δ(Cl1,O3) and δ(C2,O3) in **2*g*** could be interpreted in favor of the stereoelectronic model. Nevertheless, the delocalized population of O3 also increases (as its total electron population also does), which is not totally expected according to SM. We also notice that replacement of fluorine with chlorine implies a larger variation in DIs, and once again, this effect can be related to the polarizability of the chlorine basin.

4. CONCLUSIONS

QTAIM electron density analysis and energy partitioning based on this method were applied to study the origin of the *gauche* conformational preference of fluoromethanol and chloromethanol. The results allow us to reach the following conclusions.

(1) The evolution of atomic electron populations along the *gauche*−*anti* anticonversion experienced by these compounds is not totally in line with the predictions of the stereoelectronic model (SM). Thus, QTAIM provides an alternative interpretation for the anomeric effect in these systems.

(2) Variation in delocalization indices does not follow the SM predictions. Moreover, the delocalized population of the

Table 8. Relative Atomic Basin Delocalization Indices $\Delta\delta(\Omega,\Omega')$ (with regard to 2*a*) in 2*g* from CCSD/6-311++(2d,2p) 6d Electron Densities Obtained through the Müller 2-RDM[a]

	Cl1	C2	O3	H4	H5	H6	$\Delta N^{del}(\Omega)$
Cl1	74.5						−16.5
C2	−40.8	−21.4					−16.1
O3	12.7	12.0	14.5				4.4
H4	−4.7	0.8	−11.3	−4.6			−4.5
H5	2.6	−1.2	0.9	0.6	−4.5		0.2
H6	−2.9	−2.9	−5.6	5.5	−2.4	−22.3	−4.2

[a]In the last column, the relative delocalized electron population for each basin, $\Delta N^{del}(\Omega)$, is also shown. All the values are in atomic units and multiplied by 10^3.

dx.doi.org/10.1021/jp310534x | J. Phys. Chem. A 2013, 117, 1641−1650

oxygen basin increases in the *gauche* arrangement (with regard to the *anti* one).

(3) The electron density of a certain methylene H decreases as its atomic basin approaches the electron density associated with oxygen lone pairs. This electron density is, basically, transferred to heavy atom basins (C and O in fluoromethanol and Cl and O in chloromethanol), increasing their atomic electron populations, in a manner similar to what had been previously found in O−C−O, O−C═O, and N−C−N compounds.

(4) The following conclusions were reached using QTAIM-based energy partitioning in fluoromethanol.

(a) The interaction between F and hydroxylic H has been obtained as the main contribution to the lower energy of the *syn* arrangement (with regard to the *anti* one), as it was previously found for the *gg* and *Z* conformational preferences in methanediol and formic acid, respectively. However, when we move to the *gauche* conformer (from the *syn* one), this interaction becomes destabilizing, while the C−O interaction plays a major stabilizing role (making it the most important one when the energies of the *anti* and *gauche* rotamers are compared).

(b) The chief interactions that stabilize the *gauche* conformer do not rely on the exchange energies, the only ones that can be related to effects without classical physical meaning, as the ones arising from the stereoelectronic model (hyperconjugation). When variations of exchange and electrostatics terms are collected separately for the whole molecule, we notice that, for *gauche* stabilization, the variation in exchange energy is smaller than that in electrostatic energy, but the former is certainly not negligible. Moreover, the relative role of exchange energy increases for rigid rotation.

(c) According to ΔV_X values, FC···O bond delocalization acquires a more important role in the rigid rotation step. However, the stabilizing effect of the FC···O bond interaction energy $[\Delta V_{int}(FC,O)]$ increases in the nuclear relaxation (and not in the rigid rotation), where $\Delta V_X(FC,O)$ is, certainly, negligible.

■ ASSOCIATED CONTENT

Supporting Information

Plots of $\Delta N(\Omega)$ and $\Delta E(\Omega)$ values obtained with CCSD versus those obtained at HF, B3LYP, and MP2 levels, potential energy curves for internal rotation computed at diverse computational levels, graphics with electron density deformation, $\Delta N(\Omega)$ and $\Delta E(\Omega)$ relative values computed at the CCSD level along the internal rotation, and detailed geometries computed for molecules **1** and **2** as well as QTAIM-based energy partitioning terms for **1***a* → **1***r* and **1***r* → **1***g* processes. This material is available free of charge via the Internet at http://pubs.acs.org.

■ AUTHOR INFORMATION

Notes

The authors declare no competing financial interest.

■ ACKNOWLEDGMENTS

We are indebted to Centro de Supercomputación de Galicia for the allocation of computational resources and to "Xunta de Galicia" for funding this research through Project INCITE08P-XIB314224PR. D.F.-C. also thanks the Spanish Ministry of Education for an FPU fellowship.

■ REFERENCES

(1) Kirby, J. *The Anomeric Effect and Related Stereoelectronic Effects at Oxygen*; Springer-Verlag: New York, 1983.
(2) Thacher, G. R. J. *The Anomeric Effect and Associated Steroelectronic Effects*; ACS Symposium Series 539; American Chemical Society: Washington, DC, 1993.
(3) Juaristi, E.; Cuevas, G. *The Anomeric Effect*; CRC Press: Boca Raton, FL, 1995.
(4) Edward, J. T. *Chem. Ind. (London, U.K.)* **1955**, 1102−1104.
(5) Anderson, C. B.; Sepp, D. T. *J. Org. Chem.* **1967**, *32*, 607−611.
(6) Romers, C.; Altona, C.; Buys, H. R.; Havinga, E. *Top. Stereochem.* **1969**, *4*, 39−97.
(7) Reed, A. E.; Curtiss, L. A.; Weinhold, F. *Chem. Rev.* **1988**, *88*, 899−926.
(8) Cooper, D. L., Ed. *Theoretical and Computational Chemistry: Valence Bond Theory*; Elsevier: Amsterdam, 2002.
(9) Bader, R. F. W. *Chem. Rev.* **1991**, *91*, 893−928.
(10) Bader, R. F. W. *Atoms in Molecules. A Quantum Theory*; International Series of Monographs in Chemistry 22; Oxford University Press: Oxford, U.K., 1990.
(11) Salzner, U.; Schleyer, P. v. R. *J. Am. Chem. Soc.* **1993**, *115*, 10231−10236.
(12) Petillo, P. A.; Lerner, L. E. In *The Anomeric Effect and Associated Stereoelectronic Effects*; Thatcher, G. J. R., Ed.; ACS Symposium Series 539; American Chemical Society: Washington, DC, 1993; Chapter 9.
(13) Salzner, U.; Schleyer, P. v. R. *J. Org. Chem.* **1994**, *59*, 2138−2155.
(14) Carballeira, L.; Pérez-Juste, I. *J. Comput. Chem.* **2000**, *21*, 462−477.
(15) Mo, Y. *Nat. Chem.* **2010**, *2*, 666−671.
(16) Werstiuk, N. H.; Laidig, K. E.; Ma, J. In *Anomeric Effect and Associated Stereoelectronic Effects*; Thatcher, G. J. R., Ed.; ACS Symposium Series 539; American Chemical Society: Washington, DC, 1993; Chapter 10.
(17) Vila, A.; Mosquera, R. A. *J. Comput. Chem.* **2007**, *28*, 1516−1530.
(18) Vila, A.; Mosquera, R. A. *Chem. Phys. Lett.* **2007**, *443*, 22−28.
(19) Eskandari, K.; Vila, A.; Mosquera, R. A. *J. Phys. Chem. A* **2007**, *111*, 8491−8499.
(20) Bader, R. F. W.; Streitwieser, A.; Neuhaus, A.; Laidig, K. E.; Speers, P. *J. Am. Chem. Soc.* **1996**, *118*, 4959−4965.
(21) Bickelhaupt, F. M.; Baerends, E. J. *Angew. Chem., Int. Ed.* **2003**, *42*, 4183−4188.
(22) Weinhold, F. *Nature* **2001**, *411*, 539−541.
(23) Ferro-Costas, D.; Otero, N.; Graña, A. M.; Mosquera, R. A. *J. Comput. Chem.* **2012**, *33*, 2533−2543.
(24) Smits, G. F.; Krol, M. C.; Altona, C. *Mol. Phys.* **1988**, *65*, 513−529.
(25) Roohi, H.; Ebrahimi, A. *THEOCHEM* **2005**, *726*, 141−148.
(26) Schneider, W. F.; Nance, B. I.; Wallington, T. J. *J. Am. Chem. Soc.* **1995**, *117*, 478−485.
(27) Radom, L.; Hehre, W. J.; Pople, J. A. *J. Am. Chem. Soc.* **1971**, *93*, 289−300.
(28) Wolfe, S.; Rauk, A.; Tel, L. M.; Csizmadia, I. G. *J. Chem. Soc. B* **1971**, 136−145.
(29) Omoto, K.; Marusaki, K.; Hirao, H.; Imade, M.; Fujimoto, H. *J. Phys. Chem. A* **2000**, *104*, 6499−6504.
(30) Frisch, M. J.; Trucks, G. W.; Schlegel, H. B.; Scuseria, G. E.; Robb, M. A.; Cheeseman, J. R.; Scalmani, G.; Barone, V.; Mennucci, B.; Petersson, G. A.; et al. *Gaussian 09*, revision A.02; Gaussian, Inc.: Wallingford, CT, 2009.
(31) Biegler-König, F. W.; Bader, R. F. W.; Tang, T.-H. *J. Comput. Chem.* **1982**, *13*, 317−328.
(32) Blanco, M. A.; Martín Pendás, A.; Francisco, E. *J. Chem. Theory Comput.* **2005**, *1*, 1096−1109.
(33) Rousseau, B.; Peeters, A.; Van Alsenoy, C. *Chem. Phys. Lett.* **2000**, *324*, 189−194.
(34) Bader, R. F. W.; Streitwieser, A.; Neuhaus, A.; Laidig, K. E.; Speers, P. *J. Am. Chem. Soc.* **1996**, *118*, 4959−4965.

(35) Müller, A. M. K. *Phys. Lett.* **1984**, *105A*, 446−452.
(36) Buijse, M. A.; Baerends, E. J. *Mol. Phys.* **2002**, *100*, 401−421.
(37) Perrin, C. L.; Armstrong, K. B.; Fabian, M. A. *J. Am. Chem. Soc.* **1994**, *116*, 715−722.